Oligosaccharyltransferase is involved in targeting to ER-associated degradation

Marina Shenkman[1,2], Navit Ogen-Shtern[1,3], Chaitanya Patel[1,2], Bella Groisman[1], Metsada Pasmanik-Chor[4], Sonya M. Schermann[5,6], Roman Körner[5] and Gerardo Z. Lederkremer[1,2,] *

[1]The Shmunis School of Biomedicine and Cancer Research, Cell Biology Division, George Wise Faculty of Life Sciences, Tel Aviv University, Tel Aviv 69978, Israel

[2]Sagol School of Neuroscience, Tel Aviv University, Tel Aviv 69978, Israel

[3]Present address: The Skin Research Institute, The Dead-Sea and Arava Science Centre, Masada 86910, Israel

[4]Bioinformatics Unit, George Wise Faculty of Life Sciences, Tel Aviv University, Tel Aviv 69978, Israel

[5]Max Planck Institute of Biochemistry, Martinsried D-82152, Germany.

[6]Ascend Advanced Therapies, Martinsried, Germany.

* Corresponding author: Gerardo Z. Lederkremer

Email: gerardol@tauex.tau.ac.il

Classification: Biological Sciences, Cell Biology

Keywords: endoplasmic reticulum/ ERAD/ HRD1/ OST/ retrotranslocation.

Abstract

The majority of membrane and secretory proteins undergo N-glycosylation, a process catalyzed by oligosaccharyltransferase (OST), a membrane-bound protein complex that associates with the translocation channels within the endoplasmic reticulum (ER). Proteins failing quality control undergo ER-associated degradation (ERAD) by retrotranslocation to cytosolic proteasomes. Using a proteomics approach, we unexpectedly identified several OST subunits as significant interactors of a misfolded ER protein bait. Previous reports have suggested other roles for OST in addition to N-glycosylation, such as participation of the OST subunit ribophorin I in quality control. Our findings demonstrate OST engagement in ERAD of glycoproteins and non-glycosylated proteins, both affected by OST subunit overexpression and partial knockdown, which interfered with ERAD in conditions that did not affect glycosylation. We studied the effects on model misfolded type I and II membrane-bound proteins, BACE476 and asialoglycoprotein receptor H2a respectively, and on a soluble luminal misfolded glycoprotein, α1-antitrypsin NHK variant. OST appears to be involved in late ERAD stages, interacting with the E3 ligase HRD1 and impacting retrotranslocation. We discuss the possibility that OST, harboring multiple transmembrane domains, might assist retrotranslocation by contributing to membrane distortion for protein dislocation.

Significance statement

About thirty percent of cellular proteins undergo processing through the endoplasmic reticulum (ER), with most being glycosylated on asparagine residues in a process called N-glycosylation. In this process, oligosaccharyltransferase (OST), an ER membrane-bound protein complex, transfers sugar chains to the protein. Here we elucidate an additional role of OST, in targeting misfolded proteins to ER-associated degradation (ERAD), a process that requires their transport from the ER to the cytosol. Employing a mass spectrometry proteomics approach, we observed differential binding of OST subunits to accumulated misfolded protein molecules following inhibition of their degradation. Interference with OST activity in conditions where its function in N-glycosylation was not affected, resulted in ERAD inhibition.

Introduction

Secretory proteins are translocated into the endoplasmic reticulum (ER), where they undergo folding and quality control. Molecules that are terminally misfolded are retrotranslocated to the cytosol to be polyubiquitinated and degraded by proteasomes, in a process known as ER-associated degradation (ERAD) (1, 2). The precise mechanism of retrotranslocation remains a subject of ongoing study. It appears that various mechanisms may exist for different ERAD substrates, contingent upon the specific E3 ubiquitin ligase involved. Among these ligases, the most well-characterized participant in ERAD is HRD1, which forms a large protein complex mediating retrotranslocation (3, 4). Studies using genetic screens in yeast identified ERAD complexes involving HRD1 (5). Subsequently, analogous components were found in mammals, including HRD1 itself (6). The primary constituents of the mammalian HRD1 complex encompass transmembrane proteins such as Derlin 1-3, Herp, and Ubxd8, along with SEL1L, OS9, and XTP3-B on the luminal side. On the cytosolic side, components include Ubc6 or Ube2G2, p97, and NGLY1 (3, 5). Structural insight into the HRD1 complex has been reported in yeast but not yet in mammalian cells (7, 8). Cryo-electron microscopy (CryoEM) studies of the yeast HRD1/HRD3 complex indicated a direct role in retrotranslocation (7). Further evidence involves *in vitro* reconstitution experiments suggesting a regulation of retrotranslocation by HRD1 autoubiquitination (9, 10). Herp, a protein tethered to the ER membrane via a hydrophobic hairpin, with most of the protein on the cytosolic side, was shown to recruit HRD1 and misfolded proteins for ERAD at a specialized ER subcompartment, the ERQC (11, 12).
An approach used to delineate the HRD1 complex and discover new components has been the pull-down of the complex through known ERAD components, such as Yos9 in yeast (13) and SEL1L (14), XTP-3B, HRD1, UBXD8, Derlin-1/2 and OS-9 in mammalian cells (15). The caveat is that overexpression affects the function and interactions of these proteins. Furthermore, even

when tagged by knock-in at the endogenous level the isolated complexes might be non-functional (16). This is because these complexes might be dormant, partial complexes, given the dynamic nature of complex assembly, influenced by the presence of an ERAD substrate (11, 17). Here we have used a SILAC (stable isotope labeling by amino acids in cell culture) proteomics approach to capture functional ERAD components. We accomplish this by pull-down of an ERAD substrate and analyzing its preferential interactors under conditions favoring the accumulation of molecules targeted for retrotranslocation and subsequent proteasomal degradation. Surprisingly, among the most highly enriched interactors were several subunits of the oligosaccharyltransferase (OST) complex.

OST plays a pivotal role in N-glycosylation, the primary post-translational modification of secretory proteins. It transfers a conserved oligosaccharide from a lipid-linked glycan donor to asparagine residues in defined sequons in newly-synthesized proteins. In mammalian cells, the OST complex consists of a catalytic transmembrane subunit (STT3A or STT3B) along with several additional transmembrane proteins including DAD1, OST48/DDOST, TMEM258, OST4, ribophorin1, ribophorin2, and subunits interacting with STT3A (KCP2, DC2/OSTC) or STT3B (TUSC3/N33 or IAP/MAGT1) (18, 19). While the primary function of the OST complex lies in protein N-glycosylation, studies suggest the participation of OST subunits, such as ribophorin I, in protein quality control (20, 21), although the mode of action remains unclear. Here we show that OST subunits have a role in protein targeting to ERAD.

Results

Identification of OST as ERAD substrate interactor by a SILAC proteomics approach.

The proteomics approach that we devised involved making a construct of an established model ERAD substrate, H2a, with an affinity binding tag (streptavidin binding peptide, SBP) and producing a stable HEK293 cell line (SBP6) expressing this fusion protein, H2aSBP. H2a, the uncleaved precursor of human asialoglycoprotein receptor (ASGPR) H2a, has been extensively studied. H2a is a type II membrane glycoprotein, completely retained in the ER (22) and is a substrate of the HRD1 complex (11, 23). As H2a can undergo natural cleavage, generating a soluble luminal fragment, we used an uncleavable mutant, H2aG78R (24). The use of the 38 amino acid SBP affinity tag allows for specific and high affinity binding and elution under mild conditions, to preserve complexes (25). H2aSBP behaves like H2a in its ER retention and targeting to ERAD and H2aSBP precipitation with streptavidin beads allows coprecipitation of Derlin1, HRD1 and Fbs2, with the latter interaction being inhibited with kifunensin (23).

SBP6 cells were cultured in the presence of media containing heavy amino acids (13C(6)15N(2) lysine) to uniformly label the proteins, while WT HEK293 cells were grown with normal light amino acids, or vice versa (Fig. 1a). Cell lysates in mild non-denaturing detergent (1% digitonin) from cells with or without H2aSBP expression were mixed at a 1:1 protein ratio, followed by precipitation with streptavidin-conjugated beads and elution by competition with biotin. Eluted proteins were subjected to SDS-PAGE, digested with trypsin and identified by electrospray tandem mass spectrometry (ESI-MS/MS). This experiment was done in cells treated without or with proteasomal inhibitors to accumulate the ERAD substrate before degradation. Both cells treated with or without proteasomal inhibitors were incubated briefly with puromycin before cell lysis, to reduce the amount of proteins undergoing cotranslational translocation into the ER. Puromycin causes the termination of nascent polypeptide chains and their release into the lumen of the ER (26).

The expression of H2aSBP increased by proteasomal inhibition and more robustly by overexpression of a dominant negative RING finger mutant of HRD1, as expected for an HRD1 substrate. The mutant HRD1 coprecipitated with H2aSBP upon pull-down of the latter with streptavidin-agarose beads (Fig. 1b).

The SBP tag allowed specific and efficient elution in non-denaturing conditions with a competitive concentration of free biotin, showing many proteins coprecipitated specifically from a lysate of cells labeled with [^{35}S] met+cys in the presence of the proteasome inhibitor MG-132 (Fig. 1c). Brief treatment with puromycin before lysis did not decrease the signal of these proteins. We used mild lysis conditions (see Methods), combined with the gentle biotin elution, to enable preservation of

137 protein complexes with little or no non-specific precipitation. Silver staining of the eluates after SDS-
138 PAGE in a similar experiment showed an excellent signal to noise ratio, with only very weak bands
139 in the control without H2aSBP, except for BSA, which was used as a blocker to reduce non-specific
140 binding during the affinity pull-down. (Fig. 1d).
141 After applying the SILAC proteomics protocol (Fig. 1a), we selected as interactors only hits showing
142 >2 fold ratio of labeled/ unlabeled after normalization to the total amount of H2a-SBP (bait)
143 obtained. We then compared the results from cells treated for 4h with MG-132 and ALLN and 15
144 min with puromycin to those from cells treated only with puromycin. Gene ontology analysis showed
145 that proteasomal inhibition led to a significant enrichment for cellular functions related to the ER,
146 ER membrane and ubiquitin/proteasome processes, which were expected, and gave us confidence
147 in the approach. One of the top function enriched categories using the DAVID gene enrichment
148 tool was the OST complex (p-value=$3.13e^{-10}$), which was unexpected (Fig. 1e). A STRING
149 interaction map showed high enrichment of proteins belonging to a few categories related to protein
150 quality control: ERAD (p-value=$1.28e^{-7}$), protein folding (p-value=$1.28e^{-7}$), glycosylation (p-
151 value=$7.03e^{-10}$)(including OST and calnexin (CNX) cycle genes), unfolded protein response (UPR)
152 and vesicular transport (p-value=$8.00e^{-6}$)(Fig. 2a). This latter category perhaps relates to the
153 participation of vesicular trafficking in ERAD, which we reported recently (27).
154 Among the most significant H2aSBP interactors, with enrichment values of 2-fold or higher in
155 proteasomal inhibitor-treated cells, were most OST subunits (Table 1). This was even more
156 surprising, considering that membrane proteins, some with multiple membrane spans such as OST
157 subunits, are usually underrepresented in the MS analysis. All of these OST subunits were highly
158 enriched upon proteasomal inhibition (Fig. 2b). It should be stressed that the puromycin treatment
159 before cell lysis should have reduced interactions with newly-made translocated proteins, where
160 H2aSBP could have encountered OST, which is associated with forward translocons (28). Indeed,
161 levels of forward translocon related proteins, such as Sec61 subunits or SSRA were at similar or
162 reduced levels in samples treated with or without proteasomal inhibitor (Fig. 2b). Other enriched
163 proteins in proteasomal inhibitor-treated samples include ERAD-related genes, such as XTP3-B,
164 SEL1 and ubiquitin, calnexin cycle genes (CNX, SEP15 and UGGT1) and other relevant genes
165 such as the ER calcium pump SERCA2 and TDP43 (Fig. 2b). TDP43, normally localized in the
166 nucleus, accumulates in the cytoplasm in several diseases, including ALS, and also upon
167 proteasome inhibition (29).
168
169 **Colocalization and increased interaction of an OST subunit with the ERAD substrate upon**
170 **proteasomal inhibition.**
171 Given the increase in the pull-down of OST subunits with the ERAD substrate upon proteasomal
172 inhibition, we then analyzed whether there was any change in the cellular localization of an OST
173 subunit in relation to the ERAD substrate under these conditions. We chose to examine the OST
174 subunit Defender Against apoptotic cell Death 1 (DAD1) (30) because it was well characterized in
175 previous studies, although it was not detected in our proteomics analysis, possibly due to its low
176 abundance. GFP-DAD1 had been shown to associate with forward translocons (31). We compared
177 the localization of GFP-DAD1 to the ERAD substrate H2a linked to monomeric red fluorescent
178 protein (H2a-RFP). Both GFP-DAD1 and H2a-RFP show an ER pattern in untreated cells, although
179 with some concentration in the juxtanuclear region (Fig. 3a). Surprisingly, under proteasomal
180 inhibition with lactacystin (Lac), GFP-DAD1 accumulated together with H2a-RFP in the juxtanuclear
181 ER-derived quality control compartment (ERQC), a staging ground for ERAD (12, 24, 32), (Fig. 3b).
182 This is similar to the effect of ERAD substrate accumulation (upon proteasomal inhibition or by
183 other means) on the localization of ERAD machinery components (HRD1, Derlin-1 (23)). Several
184 ER chaperones, such as CNX and CRT, also relocalize to the ERQC under these conditions, but
185 not others, such as BiP (32, 33). As we had also seen before (24), the translocon subunit Sec61β
186 linked to GFP accumulates at the ERQC with the ERAD substrate upon proteasomal inhibition (Fig.
187 3c, d). To test whether the entire translocation complex linked to ribosomes (at the rough ER)
188 accumulates in the ERQC along with the ERAD substrate, we immunostained cells transfected with
189 H2a-RFP using an anti-ribosomal RNA (rRNA) antibody as a ribosomal marker. As opposed to
190 DAD1 and Sec61β, the ribosomes did not accumulate together with H2a-RFP after Lac treatment

191 and remained in a cytosolic and ER pattern (Fig. 3e, f). Sec61 participates in the forward
192 translocation complex, but has also been implicated in retrotranslocation (34).
193 We compared the localization of GFP-DAD1 with that of the ERAD-associated luminal lectin OS-9,
194 which appears constitutively localized mainly at the ERQC (11, 35). Similar to H2a-RFP, the GFP-
195 DAD1 that accumulated under proteasomal inhibition colocalized with OS-9 (Fig. 3 h, k). In this
196 experiment bortezomib (Bz) was used for proteasome inhibition. However, while the colocalization
197 of H2a-RFP with OS-9 increased significantly upon proteasomal inhibition, that of GFP-DAD1 did
198 not change (Fig. 3 i, l). This suggests that a portion of GFP-DAD1 molecules localize to the ERQC
199 in untreated cells and may already colocalize with OS-9 in peripheral regions.
200 We used iodixanol gradients optimized to separate ER subcompartments as a different approach
201 to analyze the localization of these proteins in relation to the ERQC (11, 36). As we had seen before
202 (11), H2a-RFP appeared mainly in middle fractions of the gradient (5-7), with a small shift to heavier
203 fractions (6-8), upon proteasomal inhibition with Bz (Fig. 3m). Endogenous DAD1 showed a similar
204 pattern in untreated cells, with a sharper accumulation in Bz-treated cells, as a peak in fraction 6,
205 and an additional smaller peak in fraction 4. Endogenous CNX and Sec61β also appeared in middle
206 fractions, partially overlapping with DAD1 in untreated conditions and in Bz-treated cells where they
207 concentrated in fraction 6. We analyzed another OST subunit, Tumor suppressor candidate 3
208 (Tusc3), a non-essential subunit that was also absent from our top proteomic hits. Endogenous
209 Tusc3 showed a similar pattern to DAD1 in untreated conditions, although concentrating more at
210 fraction 4, but it did not shift to higher densities upon proteasomal inhibition (Fig. 3m). A ribosomal
211 subunit, RPL26 appeared at higher densities, marking regions of rough ER, with little or no overlap
212 with the ERQC (Fig. 3m), as we had seen before (11).
213 A specific interaction of GFP-DAD1 and H2a was detected by coimmunoprecipitation (Fig. 4), which
214 was significantly increased upon proteasomal inhibition, suggesting that molecules targeted for
215 degradation have a higher probability of interacting than newly made ones.
216 In summary, upon proteasomal inhibition DAD1 accumulates in the ERQC, in association with an
217 ERAD substrate and separate from the rough ER, which contains forward translocons.
218
219 **OST subunits promote the degradation of glycosylated H2a and to a lesser extent of its non-**
220 **glycosylated mutant**
221 To investigate a possible role of OST in ERAD, we first overexpressed GFP-DAD1 and analyzed
222 its effect on H2a. Overexpression of GFP-DAD1 led to a dramatic decrease in the levels of H2a
223 (Fig. 5a), suggesting that the protein was degraded. There was no change in the migration of H2a,
224 indicating that glycosylation was not affected. We then partially knocked down DAD1 (Suppl. Fig.
225 1), which had a major effect in increasing the levels of H2a, suggesting that ERAD was inhibited
226 (Fig. 5b). This partial knockdown had only a very minor effect on glycosylation, as a weak band of
227 faster migration appeared suggesting the existence of a small population of underglycosylated
228 molecules (2 of the 3 glycosylation sites occupied according to our previous studies (37)). We then
229 tried partially knocking down Tusc3 (Suppl. Fig. 1), which also caused a major accumulation of H2a
230 (Fig. 5c). Tusc3 is a non-essential OST subunit, but nevertheless also caused the appearance of
231 a minor population of underglycosylated H2a molecules. Therefore, partial knockdown of DAD1 or
232 Tusc3, in conditions that affect minimally OST function in glycosylation, have a major effect on
233 inhibiting ERAD.
234 To confirm that the effects on the steady state levels of H2a were due to changes in its degradation,
235 we performed pulse-chase analysis experiments using [^{35}S] cys metabolic labeling. The
236 overexpression of GFP-DAD1 led to a significantly accelerated degradation of H2a (Fig. 5d).
237 Conversely, knockdown of Tusc3 strongly slowed down the degradation (Fig. 5e).
238 Although glycosylation of H2a did not seem to be affected, we wanted to test whether the effect of
239 Tusc3 knockdown on H2a degradation could be due to inhibition of N-glycosylation of key
240 components of quality control or ERAD. To test this, we inhibited completely N-glycosylation by a
241 long (18h) incubation of cells with tunicamycin (Tun), after which we performed a pulse-chase
242 experiment in the presence of Tun. The treatment caused a shift in the migration of H2a due to lack
243 of its 3 N-glycan chains (Fig 5f). However, the rate of H2a degradation showed no significant
244 change in the presence of Tun (Fig 5f graph), which suggests that the effect of Tusc3 knockdown

in delaying degradation (Fig. 5c and 5e) cannot be ascribed to inhibition of glycosylation of the ERAD substrate or of ERAD components.
Similar experiments were performed on a non-glycosylated mutant of H2a (H2aΔgly, (37)). GFP-DAD1 overexpression and Tusc3 knockdown had similar effects on H2aΔgly as on glycosylated H2a, but to a much lesser extent (compare Fig. 6 a, c, d with Fig. 5 a, c, e respectively). DAD1 knockdown did not have any effect on H2aΔgly degradation (Fig. 6b). DAD1 does not seem to participate in H2aΔgly ERAD at its endogenous levels, but can target the non-glycosylated protein when DAD1 is overexpressed.

OST subunits participate in ERAD of other membrane and luminal substrates

To test whether OST subunits are more generally involved in ERAD, we analyzed other well-established ERAD substrates, BACE476, a mutant type I membrane-bound glycoprotein (in contrast with H2a, which is type II, (11)) and the soluble luminal misfolded glycoprotein human α1-antitrypsin variant null Hong Kong (NHK) (38). Overexpression of GFP-DAD1 led to a decrease in the levels of BACE476 and NHK, although to a much lesser extent than for H2a (compare Fig. 7 a, d to Fig. 5). Similarly, DAD1 or Tusc3 knockdown caused an accumulation of BACE476 and NHK but again less pronounced than for H2a (compare Fig. 7 b, c, e, f to Fig. 5).
Thus, OST subunits can promote ERAD of type I or type II transmembrane substrates and of a soluble luminal substrate, but with some differences in the extent of their action depending on the substrate.

Interaction between DAD1 and HRD1 and promotion of retrotranslocation by OST subunits

As the ERAD substrates used in our experiments are targeted to HRD1, we wondered whether DAD1 and HRD1 interact. In a coimmunoprecipitation experiment, we could see a robust and specific interaction between GFP-DAD1 and HRD1-myc (Fig. 8a). Although both DAD1 and HRD1 accumulated upon proteasomal inhibition, the ratio of DAD1 coimmunoprecipitated in association with HRD1 decreased (Fig. 8a graph). This suggests that possibly DAD1 associates with HRD1 in a functional ER membrane complex and does not interact with HRD1 molecules that are already targeted for proteasomal degradation.
We next studied the requirement of OST subunits for the retrotranslocation step. We tested the effect of manipulating the levels of OST subunits on retrotranslocation using the BAP/BirA system (39). This system utilizes the E. coli biotin ligase BirA expressed in the cytosol of mammalian cells to specifically biotinylate a 15 amino acid biotin-acceptor peptide (BAP). Secretory proteins with a BAP tag on their ER luminal side are biotinylated only after retrotranslocation. A construct of H2a with BAP attached to its luminal C-terminus behaved consistently as expected for a type II membrane protein (40). H2a-BAP was biotinylated poorly when coexpressed with cytosolic BirA, but to a much higher extent when coexpressed with a luminally expressed secBirA, which contains a signal peptide for translocation into the ER (39) (Fig. 8b). There was no biotinylation in a control without BirA or secBirA. As BAP is on the luminal C-terminus of H2a, it can be exposed to the cytosolic BirA only after H2a-BAP retrotranslocation. Overexposure of the cytosolic biotinylated retrotranslocated H2a signal allowed us to assess the effect of overexpression or knockdown of OST subunits (Fig. 8c). GFP-DAD1 overexpression caused a decrease in total H2aBAP, as observed for H2a (Fig. 8c lower panel, compared to Fig. 5a), but there was a much smaller decrease in retrotranslocated biotinylated H2aBAP (Fig. 8c upper panel), resulting in a large increase in the ratio of retrotranslocated molecules relative to total, as compared to the control (Fig. 8c graph). Knockdown of either DAD1 or Tusc3 had the opposite effect, resulting in a significant decrease in the retrotranslocation ratio compared to the control.
Together, these results suggest that OST interacts with HRD1 and participates in the retrotranslocation process towards ERAD (Fig. 8d).

Discussion

In the present study we aimed to identify ERAD machinery components through their interaction with a model misfolded protein being targeted to this pathway. For this aim, we developed an approach for isolation of functional protein complexes engaged in the retrotranslocation event,

300 under conditions in which there is enrichment in retrotranslocation complexes, while minimizing the
301 abundance of forward translocons. This approach employed proteasomal inhibition to accumulate
302 the ERAD substrate just prior to degradation. Our previous studies with H2a, the model substrate
303 used, indicated that in these conditions H2a accumulates in the ERQC membrane, because its
304 retrotranslocation appears to be coupled to its degradation (11, 12, 24, 32). To reduce the presence
305 of components of the forward translocon in the protein complexes obtained, we incubated the cells
306 with puromycin. This antibiotic causes release of nascent chains from the ribosome and as a result
307 from the translocons. The combination of puromycin treatment with the C-terminal SBP tag used
308 as bait was intended to prevent isolation of the machineries in charge of translation and forward
309 translocation through incompletely translated H2aSBP molecules (which would lack a complete
310 SBP). In these conditions, we observed an association of several of the OST subunits along with
311 H2a in pulldown experiments. Notably, some of these subunits, OSTC, STT3A and MAGT1 were
312 detected only after proteasome inhibition (Fig. 2b); this, together with the puromycin treatment
313 suggests a preferential interaction with the ERAD substrate after its translation and translocation.
314 Consistently, coimmunoprecipitation of DAD1 occurred after full glycosylation of H2a (Fig. 4).
315 OST association was reported with other ER proteins in different high MW complexes, one of them
316 containing SSRD (Trap delta) (41). Interestingly, we also detected SSRD only after puromycin
317 treatment and proteasome inhibition (Fig. 2b). Mutations in SSRD lead to defects in glycosylation
318 (42), suggesting an early cotranslational event, as the SSR/ Trap complex has been implicated in
319 forward translocation. However, an alternative role has also been suggested for this complex in
320 ERAD (43, 44). Other ER proteins have been suggested to participate in both forward translocation
321 and in retrotranslocation towards ERAD, such as calumin (CCDC47) (45), and the Sec61 complex,
322 for which interaction was found with ERAD factors (34). Consistently, we found Sec61 subunits and
323 CCDC47 at similar levels in cells with and without proteasomal inhibition (Fig. 2b). It is noteworthy
324 that TDP-43 appeared enriched in cells with proteasomal inhibition. TDP-43 is localized mainly in
325 the nucleus but has been found sequestered at the cytosolic face of the ER in ALS (46).
326 For OST, noncanonical activities have also been suggested, such as that required for Dengue virus
327 infection, which could be sustained with catalytically inactive OST subunits (47). The OST subunit
328 MAGT1 and its oxidoreductase activity (48) appeared essential for the infection. MAGT1 was
329 present as one of the most significant interactors of our substrate under proteasome inhibition (Fig.
330 2b). MAGT1 is found associated with an STT3B containing complex (49). The presence of MAGT1
331 and the effects of knockdown of Tusc3 (also associated with STT3B) would implicate the STT3B
332 complex in our study. STT3B was not detected in the proteomics results, perhaps due to low
333 abundancy, but STT3A and its associated OSTC were, suggesting also a participation of the
334 STT3A complex in ERAD (Fig. 2).
335 There are previous studies that hint to the participation of OST subunits in quality control and
336 ERAD. It was suggested that ribophorin I might be involved in protein quality control, as it interacted
337 with a quality control substrate, a fragment of the amyloid precursor protein, after its translocation,
338 remaining associated after puromycin release (21). In the case of ERAD highjacking by CMV, the
339 CMV US11 protein was found associated with OST subunits, ribophorin 1, ribophorin 2, and OST48
340 (50). The ER protein malectin forms a complex with ribophorin 1 which retains misfolded NHK α1-
341 antitrypsin and misfolded ribonuclease A but not the WT counterparts in the ER (20). In a
342 proteomics study using OS-9 as a bait, Christianson et al pulled down ribophorin 1 with high score
343 (51). They also pulled down other OST subunits, such as STT3A, STT3B and DAD1 using UbxD8,
344 Derlin-1 or Derlin-2 as baits (15). However, these observations were not further investigated.
345 Our proteomics findings, along with insights from the effects of modulating DAD1 and Tusc3 levels,
346 strongly suggest the participation of most, if not all, OST subunits in ERAD. It is likely that DAD1
347 and Tusc3 fell below the detection threshold in our proteomics analysis. Despite this, DAD1
348 exhibited clear associations with the ERAD substrate (Fig. 4) and HRD1 (Fig. 8) and showed strong
349 effects of its overexpression. The effect of overexpression of this single OST subunit on ERAD
350 might be explained by the limited quantity of its endogenous expression in relation to other subunits
351 (52). Interestingly, both DAD1 and Tusc3 partial knockdowns yielded notable impacts on ERAD
352 without any significant change in glycosylation.
353 Both DAD1 and Sec61β relocalized to the ERQC under proteasomal inhibition (Fig. 3), suggesting
354 that most of their molecules are associated with the ERQC and not with forward translocons in

these conditions. In a previous study, GFP-DAD1 had been observed to remain with relatively low mobility in the ER membrane, even after puromycin termination of protein synthesis and release from translocons. This observation led to the conclusion that GFP-DAD1 probably remains associated with inactive translocons (31). However, the low mobility after puromycin treatment (as we do here) might instead signify a population of GFP-DAD1 molecules associated with a retrotranslocation complex. Indeed, GFP-DAD1 associates with HRD1 (Fig. 8). Intriguingly, other OST subunits were reported to undergo cleavage by the intramembrane rhomboid protease RHBDL4 before being targeted to ERAD (53). Thus, if GFP-DAD1 were undergoing a similar targeting for ERAD, we would expect to observe cleaved molecules upon association with HRD1, but this was not the case.

We can only speculate, with the data that we have at the moment, about how OST precisely contributes to ERAD. The fact that the OST complex encompasses many transmembrane domains, interacts with HRD1 and affects retrotranslocation suggests that it may participate directly in the mechanism of retrotranslocation. It might contribute to membrane distortion, akin to that proposed for the interphase between HRD1 and Der1 in yeast (54).

Targeting to ERAD has been best studied for glycoproteins and is linked to glycan processing and recognition steps (12). OST could be a candidate for glycan recognition and targeting to ERAD. However, OST function for ERAD does not appear to be restricted to glycoproteins, although the results of OST subunit overexpression and knockdown suggest some preference for glycosylated substrates (Fig. 5, 6). This dual targeting could be equated to the activities of OS-9, XTP3-B and EDEM1 in targeting both glycoproteins and non-glycoproteins to ERAD (37, 55, 56).

Materials and Methods

Materials

Streptavidin-agarose-beads, Biotin, tunicamycin, puromycin, MG-132, ALLN, bortezomib, digitonin were from Sigma. Lactacystin was from Cayman Chemicals (Ann Arbor, MI). Promix cell labeling mix ([35S]Met plus [35S]Cys), 1000 Ci/mmol, was from PerkinElmer Life Sciences. Predesigned shRNAs for Tusc3 (TRCN0000038065, TRCN0000038067, TRCN0000299038, TRCN0000299109, TRCN0000299107) and DAD1 (TRCN0000310240, TRCN0000200464, TRCN0000083039, TRCN0000200404, TRCN0000083041) were from Sigma.

Antibodies

Rabbit anti-DAD1, anti-Tusc3 and anti-calnexin, and mouse anti-β tubulin and anti-actin were from Sigma. Mouse anti-HA was from Biolegend and anti-Myc was custom produced and used before (35). Mouse anti-rRNA from Abcam was a kind gift of Orna Elroy-Stein. Rabbit anti-RPL26 was from Cell Signaling. Rabbit polyclonal anti-H2a carboxy-terminal and amino-terminal antibodies and mouse monoclonal anti–H2a carboxy-terminal antibody B9 were the ones used in earlier studies (11, 57). Mouse anti–S-tag was from Novagen (Gibbstown, NJ). Rabbit anti-GFP was from Santa Cruz Biotech. Rabbit anti-RFP was from MBL. Rabbit anti-Sec61β was the one used previously (32). Strep-HRP, goat anti-mouse IgG-HRP, goat anti-rabbit IgG-HRP and goat anti-mouse IgG conjugated to Cy2 or to Dylight 549 were from Jackson-Immuno-Research Labs.

Plasmids and constructs

WT HRD1-myc, dominant negative mutant hsHRD1-myc (MutHRD1-myc), Sec61β-GFP, S-tagged-OS-9.1 and S-tagged-OS-9.2 in pcDNA3.1(+), H2a and H2a mutated in its three glycosylation sites (H2aΔgly), subcloned in pCDNA1 and BACE476-HA were used before (11, 24, 36, 58), as well as human α1-antitrypsin NHK-HA in pcDNA3.1 (27). Constructs encoding H2aG78R uncleavable mutant fused through its C-terminus to a 38-amino acid streptavidin binding peptide (H2aSBP), to monomeric red fluorescent protein (H2aRFP) or to GFP (H2aGFP) were described before (11, 23, 24). DAD1 in pEGFP-C1 (GFP- DAD1) was a kind gift from Gert Kreibich. H2a-BAP-V5 was used before (40). BirA and Sec-BirA plasmids were a kind gift of Gianlucca Petris and Oscar Burrone (ICGEB, Trieste, Italy) (39).

410 **Cell culture, media and transfections**
411 NIH 3T3 and HEK293 cells were grown in DMEM supplemented with 10% bovine calf serum at 37
412 °C under 5% CO_2. Transfections of NIH 3T3 cells were carried out using a Neon MP-100
413 microporator system (Life Technologies, Carlsbad, CA). Transfection of HEK293 cells was
414 performed using the calcium phosphate method. An HEK293 stable cell line expressing H2aSBP
415 (SBP6) was described previously (23).
416
417 **BAP construct transfection and probing**
418 H2a-BAP-V5 was transfected using the calcium phosphate method in HEK293 cells together with
419 an equal amount of plasmid carrying BirA (cytosolic biotin ligase). Biotin (100μM) was added 24
420 hours post transfection overnight. The cells were then rinsed with PBS and lysed at 4˚C in Buffer
421 A (1% Triton X-100, 0.5% NaDOC and 1X cOmplete Protease Inhibitor Cocktail (Roche) in PBS),
422 containing 10mM N-ethylmaleimide, to block BirA post-lysis activity. The probing of biotinylated
423 proteins on blots was performed using Strep-HRP in PBS-TWEEN (0.5%), followed with detection
424 by enhanced chemiluminescence (ECL).
425
426 **Metabolic labeling**
427 Subconfluent (90%) cell monolayers in 60-mm dishes were labeled for 30 min with [^{35}S]Cys and
428 chased for different periods of time with normal DMEM plus 10% FCS, lysed, and
429 immunoprecipitated with anti-H2a carboxy-terminal antibody as described previously (57, 58).
430 Quantitation was performed in a Fujifilm FLA 5100 phosphorimager (Tokyo, Japan).
431
432 **Immunoprecipitation, crosslinking and immunoblotting**
433 Cell lysis in buffer A and immunoprecipitation methods are described in (23). For GFP-DAD1 co-
434 expressed with H2a, crosslinking was performed with DSP prior to cell lysis. Cells were washed 2X
435 with PBS and incubated with PBS containing 1mM DSP at 4˚C for 1 hour. The reaction was stopped
436 by incubation at 4˚C for 20 min with 50mM Glycine, followed by a rinse with PBS and incubation
437 with 20mM Tris-HCl pH7.4 in PBS for at RT 5 min.
438 For precipitation with streptavidin-agarose beads, cell lysates were incubated with the beads on a
439 vertical rotating mixer at 4°C overnight. After centrifugation, the beads were washed three times
440 with 0.5% Triton X-100, 0.25% NaDOC and 0.5% SDS in PBS and once with PBS. Samples were
441 boiled in sample buffer for 5 minutes and run on SDS-PAGE under reducing conditions.
442 Transfer to a nitrocellulose membrane, immunoblotting, detection by ECL, and quantitation in a
443 Bio-Rad ChemiDocXRS Imaging System (Hercules, CA) were done as described previously (35).
444 Quantity one or ImageJ software were used for the quantitation.
445
446 **Iodixanol equilibrium sedimentation gradient**
447 Iodixanol gradients were performed similarly to previously described (27). Briefly, HEK293 cells
448 expressing H2a-RFP (untreated or treated with Bz) were washed with PBS, resuspended in a
449 homogenization buffer (0.25M Sucrose, and 10mM HEPES pH7.4). The cells were passed through
450 a 21G needle 5 times before homogenization in a Dounce homogenizer (low clearance pestle, 30
451 strokes). The homogenates were centrifuged at 1000xg for 10 minutes at 4˚C to remove nuclei and
452 cell debris and the supernatants were loaded on top of an iodixanol gradient (10 to 34%). The
453 gradients were ultra-centrifuged at 24,000 rpm (98,500g, Beckman SW41 rotor) at 4˚C for 16 hours.
454 1ml gradient fractions were collected from top to bottom, precipitated with 10% TCA and run on
455 SDS-PAGE.
456
457 **Immunofluorescence Microscopy**
458 Immunofluorescence was performed as described previously (32, 59, 60). Briefly, cells grown for
459 24 h after transfection on coverslips in 24-well plates were fixed with 3% paraformaldehyde for 30
460 min, incubated with 50mM glycine in PBS, and permeabilized with 0.5% Triton X-100. After blocking
461 with normal goat IgG in PBS/ 2% BSA, they were exposed to primary antibody for 60 min, washed
462 and incubated for 30 min with a secondary antibody, followed by washes and staining of nuclei with
463 DAPI. Specimens were observed on a Zeiss laser scanning confocal microscope (LSM 510; Carl
464 Zeiss, Jena, Germany). ImageJ was used to quantify fluorescence intensity and to calculate

465 Mander's coefficients (using JACOP) for colocalization studies. ERQC localization was determined
466 by the accumulation of H2a fluorescent fusion proteins or of OS-9.
467
468 **Proteomics**
469 SBP binding and elution conditions were as in (61)). For SILAC proteomics HEK293 or SBP6 cells
470 were labeled with 13C(6)15N(2) L-lysine for 10 days. The labeling efficiency obtained was 97%.
471 $7x10^8$ cells (15x150mm dishes) were treated with or without 50μM MG-132 + 50μM ALLN for 4h
472 and with 2mM puromycin for the last 15min before lysis. Cells were lysed in 1% digitonin in
473 PBS+2mM PMSF+5μg/ml aprotinin. Labeled HEK293 and unlabeled SBP6 lysates were mixed at
474 a 1:1 protein ratio. The combined lysates were subjected to ON precipitation with preblocked
475 streptavidin beads (0.5% BSA, 0.2% digitonin in PBS for 2-3 h, washed once with 0.1% BSA in the
476 same buffer composition). Precipitation was with beads in 0.1% BSA, 0.2% digitonin in PBS,
477 followed by 4 washes with 0.2% digitonin in PBS and protein interactors pulled down with H2aSBP
478 were eluted for 1h at +4°C by competition with 250μM free biotin dissolved in the wash buffer.
479 Samples were heated at 65°C with β-mercapto-ethanol containing sample buffer for 10min and run
480 on SDS-PAGE. Proteins were identified by nano LC-MS/MS using a nanoACQUITY UPLC nano
481 liquid chromatography system (Waters) coupled to a LTQ orbitrap mass spectrometer (Thermo) or
482 an EasyLC system (Proxeon) coupled to a Thermo LTQ-FT Ultra mass spectrometer. For nanoLC
483 peptide separation, 15 cm long capillary column (75 µm inner diameter) with a prepulled capillary
484 tip (Proxeon) were packed in-house with Reprosil-Pur 3 µm C18 material (Dr. Maisch). Peptides
485 were eluted at 0.3 µl/min using stepwise gradients from 2%–60% acetonitrile, in 0.1% formic acid.
486 MS/MS analysis on the LTQ orbitrap mass spectrometer was performed with standard settings
487 using cycles of 1 high resolution MS scan from m/z 370-1750 followed by MS/MS scans of the 10
488 most intense ions with charge states of 2 or higher. For analysis on the Thermo LTQ-FT Ultra mass
489 spectrometer, FT scans from m/z 400-2000 were taken at 100,000 resolution, followed by collision
490 induced dissociation (CID) scans in the LTQ of the 8 most intense ions with signal greater than
491 2000 counts, and charge state of 2 or higher.
492
493 **Bioinformatics analysis**
494 Protein identification and SILAC based quantitation was performed with MaxQuant (version
495 1.0.13.13) using default settings. The UNIPROT human database (version 2009-04-14) was used
496 for protein identification. MaxQuant uses a decoy version of the specified UNIPROT database to
497 adjust the false discovery rates for proteins and peptides to below 1%.
498 Gene ontology enrichment of 86 differentially expressed proteins was performed using DAVID tool
499 (62). Selected enriched functions were presented. Differentially expressed proteins were applied
500 to STRING protein-interaction tool (63). Protein colors represent enriched functions circled in
501 colors.
502
503 **Statistical Analysis**
504 The results are expressed as average ± SD. Student's t-test (two-tailed) was used to compare the
505 averages of two groups. Statistical significance was determined at P<0.05 (*), P<0.01 (**), P<0.001
506 (***).
507

508

509 **Acknowledgments**
510
511 We would like to thank G. Kreibich, O. Elroy-Stein, G. Petris and O. Burrone for plasmids and
512 reagents. We are very grateful to F.U. Hartl for ongoing advice and for critically reading and helping
513 in the edition of this manuscript. Work was supported by grant 2577/20 from the Israel Science
514 Foundation (GZL).
515
516 **Author Contributions:** Conceptualization: GZL. Investigation: MS, NO-S, CP, BG, S.S., RK.
517 Bioinformatics: MPC. Supervision: GZL. Writing: GZL. Review and editing: GZL, MS, MPC, RK.

518
519 **Declaration of Interests:** The authors declare no competing interests.

520
521 **References**
522

523 1. Sun Z & Brodsky JL (2019) Protein quality control in the secretory pathway. *J Cell Biol*
524 218(10):3171-3187.
525 2. Wu X & Rapoport TA (2018) Mechanistic insights into ER-associated protein
526 degradation. *Curr Opin Cell Biol* 53:22-28.
527 3. Christianson JC, Jarosch E, & Sommer T (2023) Mechanisms of substrate processing
528 during ER-associated protein degradation. *Nat Rev Mol Cell Biol* 24(11):777-796.
529 4. Lopata A, Kniss A, Löhr F, Rogov VV, & Dötsch V (2020) Ubiquitination in the ERAD
530 Process. *Int J Mol Sci* 21(15).
531 5. Berner N, Reutter KR, & Wolf DH (2018) Protein Quality Control of the Endoplasmic
532 Reticulum and Ubiquitin-Proteasome-Triggered Degradation of Aberrant Proteins: Yeast
533 Pioneers the Path. *Annu Rev Biochem* 87:751-782.
534 6. Kikkert M*, et al.* (2004) Human HRD1 is an E3 ubiquitin ligase involved in degradation of
535 proteins from the endoplasmic reticulum. *J Biol Chem* 279(5):3525-3534.
536 7. Schoebel S*, et al.* (2017) Cryo-EM structure of the protein-conducting ERAD channel
537 Hrd1 in complex with Hrd3. *Nature* 548(7667):352-355.
538 8. Wu X*, et al.* (2020) Structural basis of ER-associated protein degradation mediated by
539 the Hrd1 ubiquitin ligase complex. *Science* 368(6489).
540 9. Peterson BG, Glaser ML, Rapoport TA, & Baldridge RD (2019) Cycles of
541 autoubiquitination and deubiquitination regulate the ERAD ubiquitin ligase Hrd1. *Elife* 8.
542 10. Vasic V*, et al.* (2020) Hrd1 forms the retrotranslocation pore regulated by auto-
543 ubiquitination and binding of misfolded proteins. *Nat Cell Biol* 22(3):274-281.
544 11. Leitman J*, et al.* (2014) Herp coordinates compartmentalization and recruitment of
545 HRD1 and misfolded proteins for ERAD. *Molecular biology of the cell* 25(7):1050-1060.
546 12. Shenkman M & Lederkremer GZ (2019) Compartmentalization and Selective Tagging for
547 Disposal of Misfolded Glycoproteins. *Trends Biochem Sci* 44(10):827-836.
548 13. Denic V, Quan EM, & Weissman JS (2006) A luminal surveillance complex that selects
549 misfolded glycoproteins for ER-associated degradation. *Cell* 126(2):349-359.
550 14. Mueller B, Klemm EJ, Spooner E, Claessen JH, & Ploegh HL (2008) SEL1L nucleates a
551 protein complex required for dislocation of misfolded glycoproteins. *Proc Natl Acad Sci*
552 *U S A* 105(34):12325-12330.
553 15. Christianson JC*, et al.* (2012) Defining human ERAD networks through an integrative
554 mapping strategy. *Nature Cell Biology* 14(1):93-105.
555 16. Hwang J*, et al.* (2017) Characterization of protein complexes of the endoplasmic
556 reticulum-associated degradation E3 ubiquitin ligase Hrd1. *J Biol Chem* 292(22):9104-
557 9116.
558 17. Kny M, Standera S, Hartmann-Petersen R, Kloetzel PM, & Seeger M (2011) Herp
559 regulates Hrd1-mediated ubiquitylation in a ubiquitin-like domain-dependent manner. *J*
560 *Biol Chem* 286(7):5151-5156.
561 18. Cherepanova N, Shrimal S, & Gilmore R (2016) N-linked glycosylation and homeostasis
562 of the endoplasmic reticulum. *Curr Opin Cell Biol* 41:57-65.

563 19. Mohanty S, Chaudhary BP, & Zoetewey D (2020) Structural Insight into the Mechanism
564 of N-Linked Glycosylation by Oligosaccharyltransferase. *Biomolecules* 10(4).
565 20. Qin SY*, et al.* (2012) Malectin forms a complex with ribophorin I for enhanced
566 association with misfolded glycoproteins. *J Biol Chem* 287(45):38080-38089.
567 21. Wilson CM*, et al.* (2005) Ribophorin I associates with a subset of membrane proteins
568 after their integration at the sec61 translocon. *J Biol Chem* 280(6):4195-4206.
569 22. Shenkman M, Ayalon M, & Lederkremer GZ (1997) Endoplasmic reticulum quality
570 control of asialoglycoprotein receptor H2a involves a determinant for retention and not
571 retrieval. *Proc Natl Acad Sci U S A* 94(21):11363-11368.
572 23. Groisman B, Shenkman M, Ron E, & Lederkremer GZ (2011) Mannose trimming is
573 required for delivery of a glycoprotein from EDEM1 to XTP3-B and to late endoplasmic
574 reticulum-associated degradation steps. *J Biol Chem* 286(2):1292-1300.
575 24. Kondratyev M, Avezov E, Shenkman M, Groisman B, & Lederkremer GZ (2007) PERK-
576 dependent compartmentalization of ERAD and unfolded protein response machineries
577 during ER stress. *Exp Cell Res* 313(16):3395-3407.
578 25. Keefe AD, Wilson DS, Seelig B, & Szostak JW (2001) One-step purification of
579 recombinant proteins using a nanomolar-affinity streptavidin-binding peptide, the SBP-
580 Tag. *Protein Expr Purif* 23(3):440-446.
581 26. Adelman MR, Sabatini DD, & Blobel G (1973) Ribosome-membrane interaction.
582 Nondestructive disassembly of rat liver rough microsomes into ribosomal and
583 membranous components. *J Cell Biol* 56(1):206-229.
584 27. Ogen-Shtern N*, et al.* (2023) COP I and II dependent trafficking controls ER-associated
585 degradation in mammalian cells. *iScience* 26(3):106232.
586 28. Pfeffer S*, et al.* (2014) Structure of the mammalian oligosaccharyl-transferase complex
587 in the native ER protein translocon. *Nat Commun* 5:3072.
588 29. Scotter EL*, et al.* (2014) Differential roles of the ubiquitin proteasome system and
589 autophagy in the clearance of soluble and aggregated TDP-43 species. *J Cell Sci* 127(Pt
590 6):1263-1278.
591 30. Kelleher DJ & Gilmore R (1997) DAD1, the defender against apoptotic cell death, is a
592 subunit of the mammalian oligosaccharyltransferase. *Proc Natl Acad Sci U S A*
593 94(10):4994-4999.
594 31. Nikonov AV, Snapp E, Lippincott-Schwartz J, & Kreibich G (2002) Active translocon
595 complexes labeled with GFP-Dad1 diffuse slowly as large polysome arrays in the
596 endoplasmic reticulum. *J Cell Biol* 158(3):497-506.
597 32. Kamhi-Nesher S*, et al.* (2001) A novel quality control compartment derived from the
598 endoplasmic reticulum. *Molecular biology of the cell* 12(6):1711-1723.
599 33. Frenkel Z, Shenkman M, Kondratyev M, & Lederkremer GZ (2004) Separate roles and
600 different routing of calnexin and ERp57 in endoplasmic reticulum quality control
601 revealed by interactions with asialoglycoprotein receptor chains. *Mol Biol Cell*
602 15(5):2133-2142.
603 34. Pereira F*, et al.* (2019) Effect of Sec61 interaction with Mpd1 on endoplasmic reticulum-
604 associated degradation. *PLoS One* 14(1):e0211180.
605 35. Ron E*, et al.* (2011) Bypass of glycan-dependent glycoprotein delivery to ERAD by up-
606 regulated EDEM1. *Molecular biology of the cell* 22(21):3945-3954.
607 36. Benyair R*, et al.* (2015) Mammalian ER mannosidase I resides in quality control vesicles,
608 where it encounters its glycoprotein substrates. *Molecular biology of the cell* 26(2):172-
609 184.

610 37. Shenkman M*, et al.* (2013) A Shared Endoplasmic Reticulum-associated Degradation
611 Pathway Involving the EDEM1 Protein for Glycosylated and Nonglycosylated Proteins. *J*
612 *Biol Chem* 288(4):2167-2178.
613 38. Lamriben L*, et al.* (2018) EDEM1's mannosidase-like domain binds ERAD client proteins
614 in a redox-sensitive manner and possesses catalytic activity. *J Biol Chem* 293(36):13932-
615 13945.
616 39. Petris G, Vecchi L, Bestagno M, & Burrone OR (2011) Efficient detection of proteins
617 retro-translocated from the ER to the cytosol by in vivo biotinylation. *PLoS One*
618 6(8):e23712.
619 40. Sharma N*, et al.* (2021) The Sigma-1 receptor is an ER-localized type II membrane
620 protein. *J Biol Chem* 297(5):101299.
621 41. Shibatani T, David LL, McCormack AL, Frueh K, & Skach WR (2005) Proteomic analysis of
622 mammalian oligosaccharyltransferase reveals multiple subcomplexes that contain
623 Sec61, TRAP, and two potential new subunits. *Biochemistry* 44(16):5982-5992.
624 42. Losfeld ME*, et al.* (2014) A new congenital disorder of glycosylation caused by a
625 mutation in SSR4, the signal sequence receptor 4 protein of the TRAP complex. *Human*
626 *Molecular Genetics* 23(6):1602-1605.
627 43. Nagasawa K, Higashi T, Hosokawa N, Kaufman RJ, & Nagata K (2007) Simultaneous
628 induction of the four subunits of the TRAP complex by ER stress accelerates ER
629 degradation. *EMBO Rep* 8(5):483-489.
630 44. Russo A (2020) Understanding the mammalian TRAP complex function(s). *Open Biol*
631 10(5):190244.
632 45. Yamamoto S*, et al.* (2014) Contribution of calumin to embryogenesis through
633 participation in the endoplasmic reticulum-associated degradation activity. *Dev Biol*
634 393(1):33-43.
635 46. Kon T*, et al.* (2022) Accumulation of Nonfibrillar TDP-43 in the Rough Endoplasmic
636 Reticulum Is the Early-Stage Pathology in Amyotrophic Lateral Sclerosis. *J Neuropathol*
637 *Exp Neurol* 81(4):271-281.
638 47. Lin DL*, et al.* (2017) Dengue Virus Hijacks a Noncanonical Oxidoreductase Function of a
639 Cellular Oligosaccharyltransferase Complex. *mBio* 8(4).
640 48. Patel C, Saad H, Shenkman M, & Lederkremer GZ (2020) Oxidoreductases in
641 Glycoprotein Glycosylation, Folding, and ERAD. *Cells* 9(9).
642 49. Cherepanova NA, Shrimal S, & Gilmore R (2014) Oxidoreductase activity is necessary for
643 N-glycosylation of cysteine-proximal acceptor sites in glycoproteins. *J Cell Biol*
644 206(4):525-539.
645 50. Lilley BN & Ploegh HL (2004) A membrane protein required for dislocation of misfolded
646 proteins from the ER. *Nature* 429(6994):834-840.
647 51. Christianson JC, Shaler TA, Tyler RE, & Kopito RR (2008) OS-9 and GRP94 deliver mutant
648 alpha1-antitrypsin to the Hrd1-SEL1L ubiquitin ligase complex for ERAD. *Nat Cell Biol*
649 10(3):272-282.
650 52. Cherepanova NA & Gilmore R (2016) Mammalian cells lacking either the cotranslational
651 or posttranslocational oligosaccharyltransferase complex display substrate-dependent
652 defects in asparagine linked glycosylation. *Sci Rep* 6:20946.
653 53. Knopf JD*, et al.* (2020) Intramembrane protease RHBDL4 cleaves
654 oligosaccharyltransferase subunits to target them for ER-associated degradation. *J Cell*
655 *Sci* 133(6).

656 54. Wu X & Rapoport TA (2021) Translocation of Proteins through a Distorted Lipid Bilayer.
657 *Trends Cell Biol* 31(6):473-484.
658 55. Hosokawa N*, et al.* (2008) Human XTP3-B forms an endoplasmic reticulum quality
659 control scaffold with the HRD1-SEL1L ubiquitin ligase complex and BiP. *J Biol Chem*
660 283(30):20914-20924.
661 56. Jaenicke LA, Brendebach H, Selbach M, & Hirsch C (2011) Yos9p assists in the
662 degradation of certain nonglycosylated proteins from the endoplasmic reticulum.
663 *Molecular biology of the cell* 22(16):2937-2945.
664 57. Tolchinsky S, Yuk MH, Ayalon M, Lodish HF, & Lederkremer GZ (1996) Membrane-bound
665 versus secreted forms of human asialoglycoprotein receptor subunits - Role of a
666 juxtamembrane pentapeptide. *J Biol Chem* 271(24):14496-14503.
667 58. Ogen-Shtern N, Avezov E, Shenkman M, Benyair R, & Lederkremer GZ (2016)
668 Mannosidase IA is in Quality Control Vesicles and Participates in Glycoprotein Targeting
669 to ERAD. *Journal of molecular biology* 428(16):3194-3205.
670 59. Avezov E, Frenkel Z, Ehrlich M, Herscovics A, & Lederkremer GZ (2008) Endoplasmic
671 reticulum (ER) mannosidase I is compartmentalized and required for N-glycan trimming
672 to Man5-6GlcNAc2 in glycoprotein ER-associated degradation. *Mol Biol Cell* 19(1):216-
673 225.
674 60. Leitman J, Ulrich Hartl F, & Lederkremer GZ (2013) Soluble forms of polyQ-expanded
675 huntingtin rather than large aggregates cause endoplasmic reticulum stress. *Nature*
676 *Communications* 4:2753.
677 61. Call ME, Pyrdol J, Wiedmann M, & Wucherpfennig KW (2002) The organizing principle in
678 the formation of the T cell receptor-CD3 complex. *Cell* 111(7):967-979.
679 62. Sherman BT*, et al.* (2022) DAVID: a web server for functional enrichment analysis and
680 functional annotation of gene lists (2021 update). *Nucleic Acids Res* 50(W1):W216-w221.
681 63. Szklarczyk D*, et al.* (2023) The STRING database in 2023: protein-protein association
682 networks and functional enrichment analyses for any sequenced genome of interest.
683 *Nucleic Acids Res* 51(D1):D638-d646.

684

685

686 **Figure legends**

687 **Fig. 1. ERAD substrate interactors identified by a SILAC proteomics approach. (a)**
688 Experimental scheme of SILAC-based mass spectrometry analysis of HEK293 cells labeled with
689 lysine containing heavy isotopes for 10 days or HEK293 stably expressing H2aSBP (SBP6 cell
690 line) without heavy lysine (or vice versa). Cells were treated with MG-132 (50μM) and ALLN
691 (50μM) for 4h and puromycin (2mM) for 15 min before lysis, or only with puromycin. Cells were
692 solubilized in 1% digitonin in PBS and lysates from cells labeled with or without heavy lysine were
693 mixed 1:1. Protein complexes pulled down with H2aSBP (using streptavidin-agarose beads) were
694 eluted with 250μM biotin, subjected to SDS-PAGE followed by trypsin digestion and LC-MS/MS
695 analysis. **(b)** Effect of mutant HRD1 on H2aSBP. Dominant negative mutant myc-tagged hsHRD1
696 (mutHRD1-myc) was transfected into SBP6 cells. Two days post-transfection these cells or
697 control HEK293 cells were treated or not for 4h with 20 μM MG132, lysed and subjected to
698 precipitation with streptavidin beads. Biotin-eluted samples were subjected to 10% SDS-PAGE
699 and immunoblotted with anti-H2a or anti-myc. MW markers in kDa are on the right. **(c)**
700 Metabolically labeled proteins pulled down with H2aSBP. SBP6 cells or control HEK293 cells
701 were labeled with [^{35}S] Cys/Met mix for 5h under proteasomal inhibition with 20mM MG132 and
702 treated or not with 2mM puromycin for the last 15 min before lysis. Cells were lysed in digitonin
703 buffer followed by precipitation with streptavidin beads, elution with biotin and SDS-PAGE with
704 detection by fluorography. **(d)** Proteins pulled down with H2aSBP and silver stained. SBP6 cells
705 or control HEK293 cells were treated for 4h with 20μM MG132 and 2mM puromycin (last 15 min),
706 lysed in digitonin buffer followed by precipitation with streptavidin beads (in the presence of 0.1%
707 BSA), elution with biotin, SDS-PAGE and silver staining. **(e)** Gene Ontology (GO) analysis of
708 differentially expressed genes from the SILAC results of cells with or without proteasomal
709 inhibition (ratio>1.5). -log2 enriched p-values are shown for selected top entries with the lowest
710 false discovery rates. (see also Suppl. Table 1)

711

712 **Fig. 2. OST subunits are among top ERAD substrate interactors. (a)** STRING interaction map
713 of proteins identified in the SILAC analysis, highlighting those with >1.5 ratio when comparing
714 cells treated with or without proteasomal inhibitors. OST protein subunits are in red, other
715 enriched functions are in colored circles. **(b)** Ratio of levels of proteins identified in cells treated
716 with or without proteasomal inhibitors. The proteins on the left (up to UBQL2) were detected only
717 in proteasomal inhibitor-treated cells. The dotted line is a value of 1, equal presence in cells
718 treated with or without proteasomal inhibitors. (see also Suppl. Tables 2 and 3).

719

720 **Fig. 3. DAD1 accumulates in the ERQC upon proteasomal inhibition separately from**
721 **ribosomes. (a-d)** GFP-DAD1 and Sec61β-GFP accumulate at the ERQC. NIH 3T3 cells were
722 transiently cotransfected with the ERAD substrate H2a-RFP and with GFP-DAD1 or Sec61β-GFP
723 and were incubated with or without 17 μM Lac for 3h. **(e-f)** Ribosomes do not accumulate at the
724 ERQC. NIH 3T3 cells transiently transfected with H2a-RFP were treated as in (a-d) and were
725 fixed and immunostained using a primary mouse anti-rRNA antibody and secondary goat anti-
726 mouse IgG antibody conjugated to Cy2. **(g-l)** GFP-DAD1 colocalizes with OS-9 with or without
727 proteasomal inhibition. S-tagged OS-9.1/2 was expressed in NIH 3T3 cells together with H2a-
728 GFP or GFP-DAD1, with or without treatment with 1.5 μM Bz for 3h, followed by fixation and
729 immunostaining with mouse anti-S tag antibody and secondary goat anti-mouse IgG antibody
730 conjugated to Dylight 549. The graphs are from data from 3 repeat experiments. **(m)** Comigration
731 of endogenous DAD1 and the ERAD substrate at the ERQC. HEK293 cells transiently transfected
732 with H2a-RFP were incubated without (left) or with Bz (2 μM) for 3 h. Cells were homogenized
733 and postnuclear supernatants were centrifuged on 10–34% iodixanol gradients. Fractions of the
734 gradients were run on SDS–PAGE and immunoblotted with the indicated antibodies. H2a-RFP
735 was detected with anti-RFP. A representative experiment out of 3 repeat experiments is shown.

736

737 **Fig. 4. Increased interaction of DAD1 with an ERAD substrate upon proteasomal inhibition.**
738 Immunoprecipitation with a mouse monoclonal (B9) anti-H2a of lysates of HEK293 cells
739 expressing H2a together with GFP-DAD1, with or without treatment with 2 μM Bz for 3 h.
740 Crosslinking with 1 mM DSP was performed before cell lysis. Immunoprecipitates and 10% of the
741 total lysates (input) were immunoblotted with rabbit anti-H2a amino-terminal antibody and anti-
742 GFP. Asterisk= non-specific band. The graph shows increased coimmunoprecipitation of GFP-
743 DAD1 with H2a upon proteasomal inhibition. Values are relative to control (=100), normalized by
744 total GFP-DAD1 and H2a, average of 4 independent experiments ±SD. p value = 0.0003.

745

746 **Fig. 5. OST subunits promote degradation of a glycosylated ERAD substrate. (a-c)**
747 Overexpression of GFP-DAD1 strongly reduces the levels of H2a, knockdown of DAD1 or Tusc3
748 increases H2a levels. Cell lysates were immunoblotted with anti-H2a amino-terminal antibody.
749 The graphs show averages of 3 or 4 independent experiments ±SD. p value ±GFP-DAD1 = $2x10^{-}$
750 ^{5}, ±shDAD1 = 0.03, ±shTusc3 = 0.0004. **(d-f)** Pulse-labeling for 20 min with [^{35}S]cysteine and
751 chase for the indicated times of cells expressing H2a with or without overexpression of GFP-
752 DAD1 (d), knockdown of Tusc3 (e) or treatment with Tun (5 μg/ml) for 18h prior to the pulse and
753 during the pulse and chase times (f). H2a degradation (percentage remaining relative to pulse)
754 was accelerated by GFP-DAD1, inhibited by Tusc3 knockdown and was not affected by blocking
755 glycosylation (+Tun). The graphs show averages of 3 independent experiments ±SD. p value
756 ±GFP-DAD1 3h = 0.05, 6h = 0.05; ±shTusc3 3h = 0.03; ±Tun 3h = 0.04.

757

758 **Fig. 6. Participation of OST subunits to a lesser extent in the degradation of an**
759 **unglycosylated ERAD substrate. (a-c)** Overexpression of GFP-DAD1 reduces the levels of
760 H2aDgly, knockdown of DAD1 does not affect its levels whereas Tusc3 knockdown increases
761 moderately H2aDgly levels. Cell lysates were immunoblotted with anti-H2a amino-terminal
762 antibody. The graphs show averages of 3 or 4 independent experiments ±SD. p value ±GFP-
763 DAD1 = $3x10^{-6}$, ±shTusc3 = 0.004. **(d)** Pulse/ chase with [^{35}S]cysteine of cells expressing
764 H2aDgly shows a moderate inhibition of its degradation by Tusc3 knockdown. The graph shows
765 an average of 3 independent experiments ±SD. p value ±shTusc3 3h = 0.01.

766

767 **Fig. 7. OST subunits affect levels of other substrates. (a-c)** Overexpression of GFP-DAD1
768 reduces moderately the levels of BACE476-HA, knockdown of DAD1 or Tusc3 cause a minor
769 increase in BACE476-HA levels. Cell lysates were immunoblotted with anti-HA and anti-actin as
770 loading control. **(d-f)** Overexpression of GFP-DAD1 causes a minor reduction in the levels of
771 NHK-HA, knockdown of DAD1 or Tusc3 increase moderately NHK-HA levels. Cell lysates were
772 immunoblotted with anti-HA and anti-β tubulin as loading control. The graphs show averages of 3
773 independent experiments ±SD. p value for BACE476-HA: ±GFP-DAD1 = 0.008, ±shDAD1 = 0.01,
774 ±shTusc3 = 0.003; for NHK-HA: ±GFP-DAD1 = 0.05, ±shDAD1 = $2x10^{-6}$, ±shTusc3 = 0.03.

775

776 **Fig. 8. Interaction of an OST subunit with HRD1 and promotion of retrotranslocation of an**
777 **ERAD substrate. (a)** Immunoprecipitation with anti-myc of lysates of HEK293 cells expressing
778 HRD1-myc together with GFP-DAD1 and treated with or without 2 μM Bz for 4 h.
779 Immunoprecipitates and 10% of the total lysates (input) were immunoblotted with anti-myc and
780 anti-GFP. The graph shows reduced coimmunoprecipitation of GFP-DAD1 with HRD1-myc under
781 proteasomal inhibition. Values are relative to control (=100), normalized by total GFP-DAD1 and
782 HRD1-myc, average of 3 independent experiments ±SD. p value = 0.009. **(b)** Scheme of addition

783 of biotin (star) to H2a-BAP by an ER luminal biotin ligase, sec-BirA or after retrotranslocation by a
784 cytosolic one, BirA. HEK293 cells transiently expressing H2a-BAP with or without BirA or Sec-
785 BirA were incubated 24h post-transfection with biotin (100μM) for 30 min before lysis. Strep-HRP
786 was used to detect biotinylated H2a-BAP and anti-V5 to detect total H2a-BAP. **(c)** Cells
787 expressing H2a-BAP together with BirA and GFP-DAD1 overexpression or knockdown of DAD1
788 or Tusc3 were incubated with biotin for 3h. Cell lysates were reacted with Strep-HRP or with anti-
789 H2a antibody. Retrotranslocated (biotinylated) H2a-BAP increased almost two-fold under GFP-
790 DAD1 overexpression and was reduced to half under Tusc3 or DAD1 knockdown. Values are
791 averages of 4 independent experiments ±SD, relative to total H2a-BAP and standardized by the
792 control (=100). P value +shTusc3 vs. control = 0.02, +GFP-DAD1 vs. control = 0.04, +shDAD1 vs.
793 control = 0.02. **(d)** Model illustrating the interaction of OST with translocon components during
794 forward translocation and its participation in N-glycosylation. OST also interacts with HRD1 and
795 participates in retrotranslocation and targeting to ERAD.

796

797 **Table 1**

798

OST subunit	**UNIPROT Accession No.**	**Hit No.**	**Median ratio with vs. without proteasome inhibition**	**Peptides (seq)**	**Sequence Coverage (%)**
IAP/ MAGT1, MAGT1_HUMAN	Q9H0U3		Only in cells treated with proteasome inhibitors	4	10.1
STT3 A, STT3A_HUMAN	P46977		Only in cells treated with proteasome inhibitors	8	11.2
DC2/ OSTC, OSATC_HUMAN	Q9NRP0		Only in cells treated with proteasome inhibitors	1	8.1
Ribophorin II, RPN2_HUMAN	P04844	27	4.3	15	30.9
OST 48, OST48_HUMAN	P39656	32	2.8	11	29.8
Ribophorin I, RPN1_HUMAN	P04843	36	2.4	18	32.5

799

800 **Table 1. OST subunits detected by mass spectrometry.** LC-MS/MS analysis following the
801 experimental scheme of Fig. 1a. Results of >2 fold labeled/unlabeled from cells treated with MG-
802 132 and ALLN for 4h and puromycin for 15 min before lysis were compared to those from cells
803 treated with only puromycin for 15 min, after normalization to the total amount of H2a-SBP
804 (ASGPR2, bait) obtained. Hits are ranked by enrichment in cells treated with vs. without
805 proteasome inhibitors. Only OST subunits, with enrichment values of 2-fold or higher in cells

806 treated with vs. without proteasome inhibitors or found only in cells treated with proteasome
807 inhibitors are shown. See Suppl. Tables 2 and 3 for complete lists of hits.

808

809

810

Fig. 1

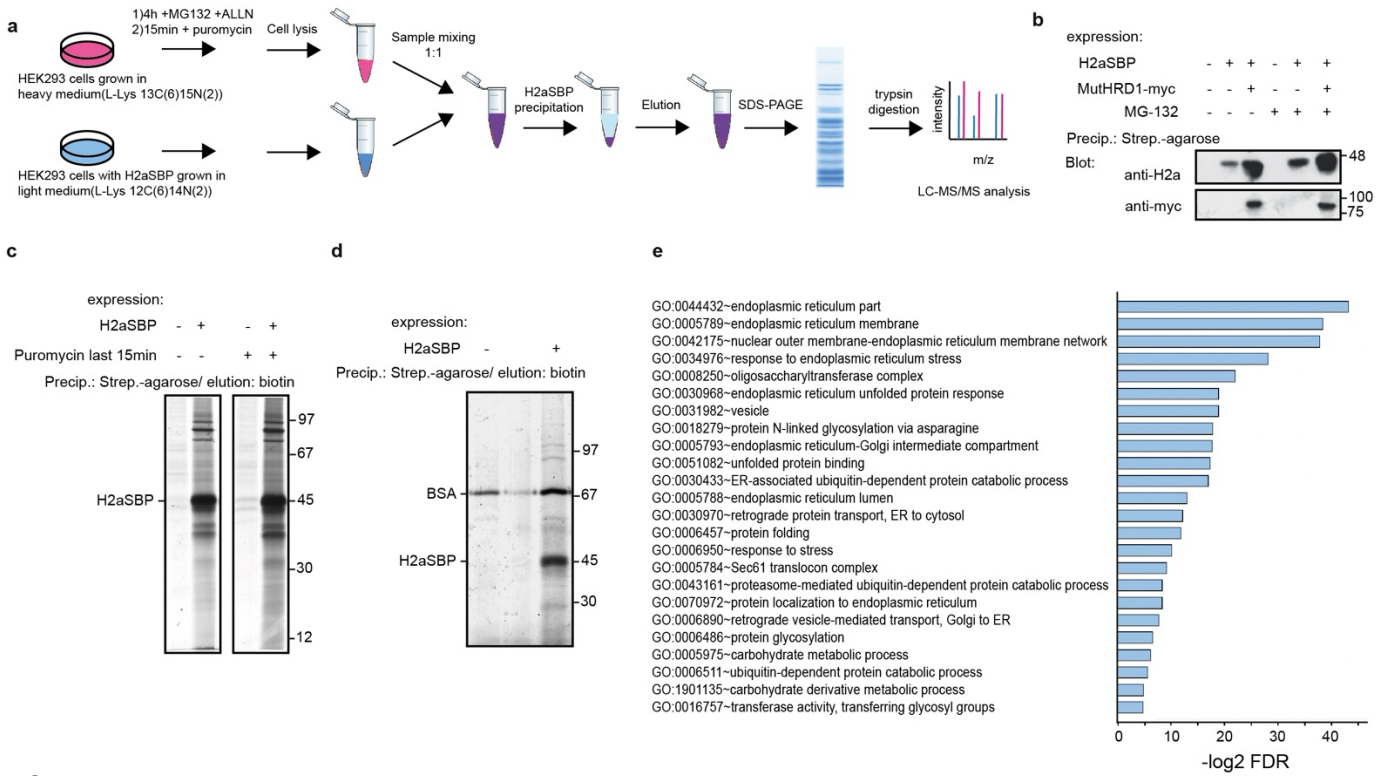

812

813

Fig. 2

a

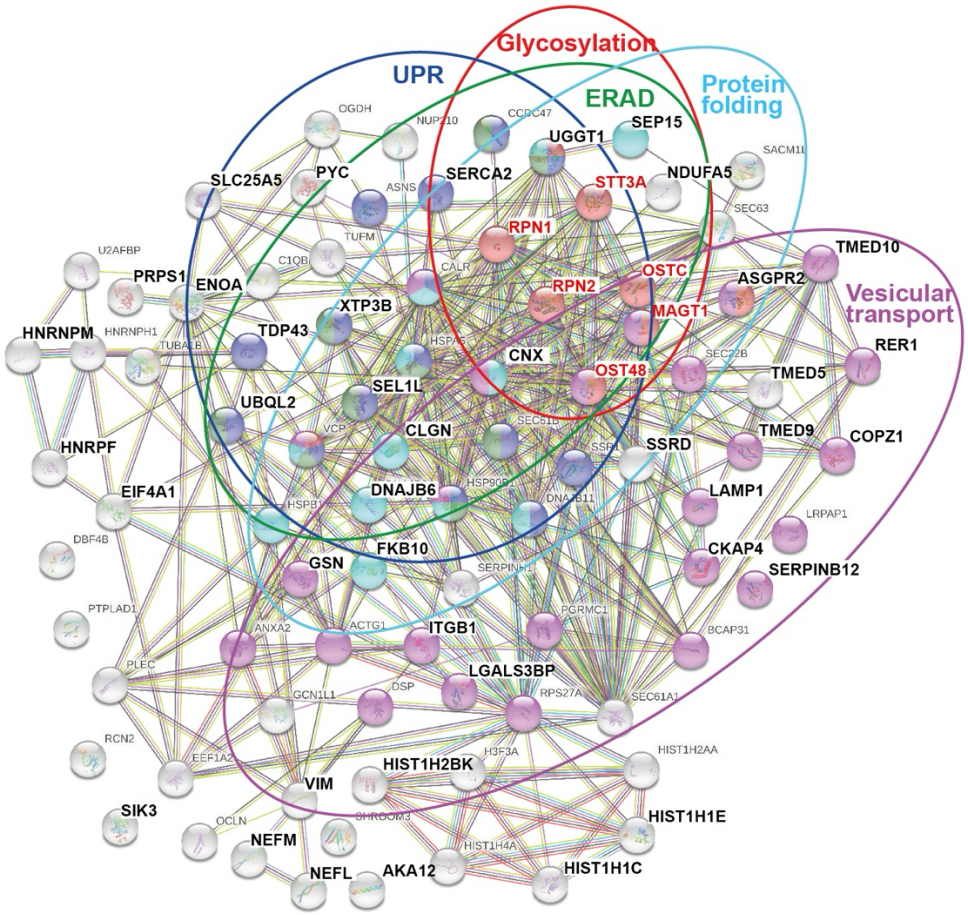
Glycosylation
UPR
ERAD
Protein folding
Vesicular transport
OGDH
NUP210
CCDC47
UGGT1
SEP15
SACM1L
SLC25A5
PYC
ASNS
SERCA2
STT3A
NDUFA5
SEC63
RPN1
TUFM
U2AFBP
C1QB
CALR
TMED10
PRPS1
ENOA
RPN2
OSTC
ASGPR2
XTP3B
MAGT1
HNRNPM
HNRNPH1
TDP43
TUBALB
HSPA5
CNX
SEC22B
RER1
OST48
TMED5
SEL1L
UBQL2
VCP
CLGN
SEC61B
TMED9
COPZ1
HNRPF
SSR1
SSRD
EIF4A1
DNAJB6
HSP90B1
DNAJB11
LAMP1
HSPB1
LRPAP1
DBF4B
FKB10
CKAP4
GSN
SERPINH1
SERPINB12
PTPLAD1
PGRMC1
ANXA2
ACTG1
ITGB1
BCAP31
PLEC
LGALS3BP
GCN1L1
DSP
RPS27A
SEC61A1
RCN2
EEF1A2
H3F3A
HIST1H2AA
HIST1H2BK
VIM
SIK3
OCLN
SHROOM3
HIST1H1E
NEFM
HIST1H4A
NEFL
AKA12
HIST1H1C

b

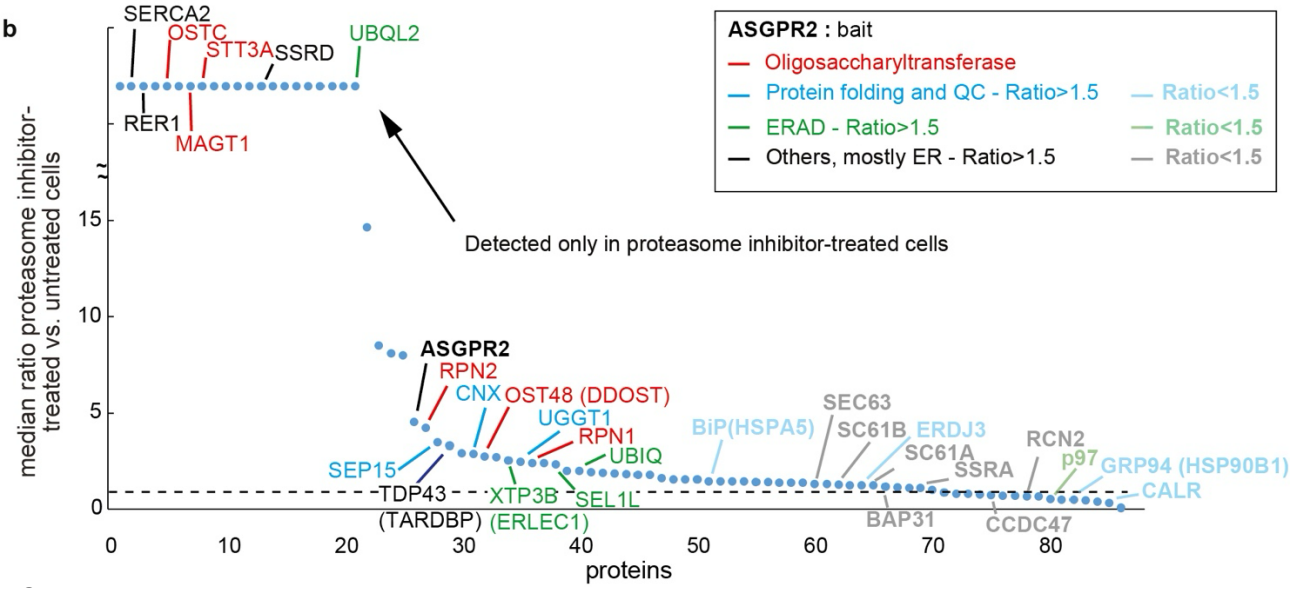
ASGPR2 : bait
Oligosaccharyltransferase
Protein folding and QC - Ratio>1.5
Ratio<1.5
ERAD - Ratio>1.5
Ratio<1.5
Others, mostly ER - Ratio>1.5
Ratio<1.5
Detected only in proteasome inhibitor-treated cells
SERCA2
OSTC
STT3A
SSRD
UBQL2
RER1
MAGT1
ASGPR2
RPN2
CNX
OST48 (DDOST)
UGGT1
RPN1
UBIQ
SEP15
TDP43
(TARDBP)
XTP3B
(ERLEC1)
SEL1L
BiP(HSPA5)
SEC63
SC61B
ERDJ3
SC61A
SSRA
BAP31
RCN2
p97
GRP94 (HSP90B1)
CALR
CCDC47
median ratio proteasome inhibitor-treated vs. untreated cells
proteins
0
5
10
15
0
10
20
30
40
50
60
70
80

Fig. 3

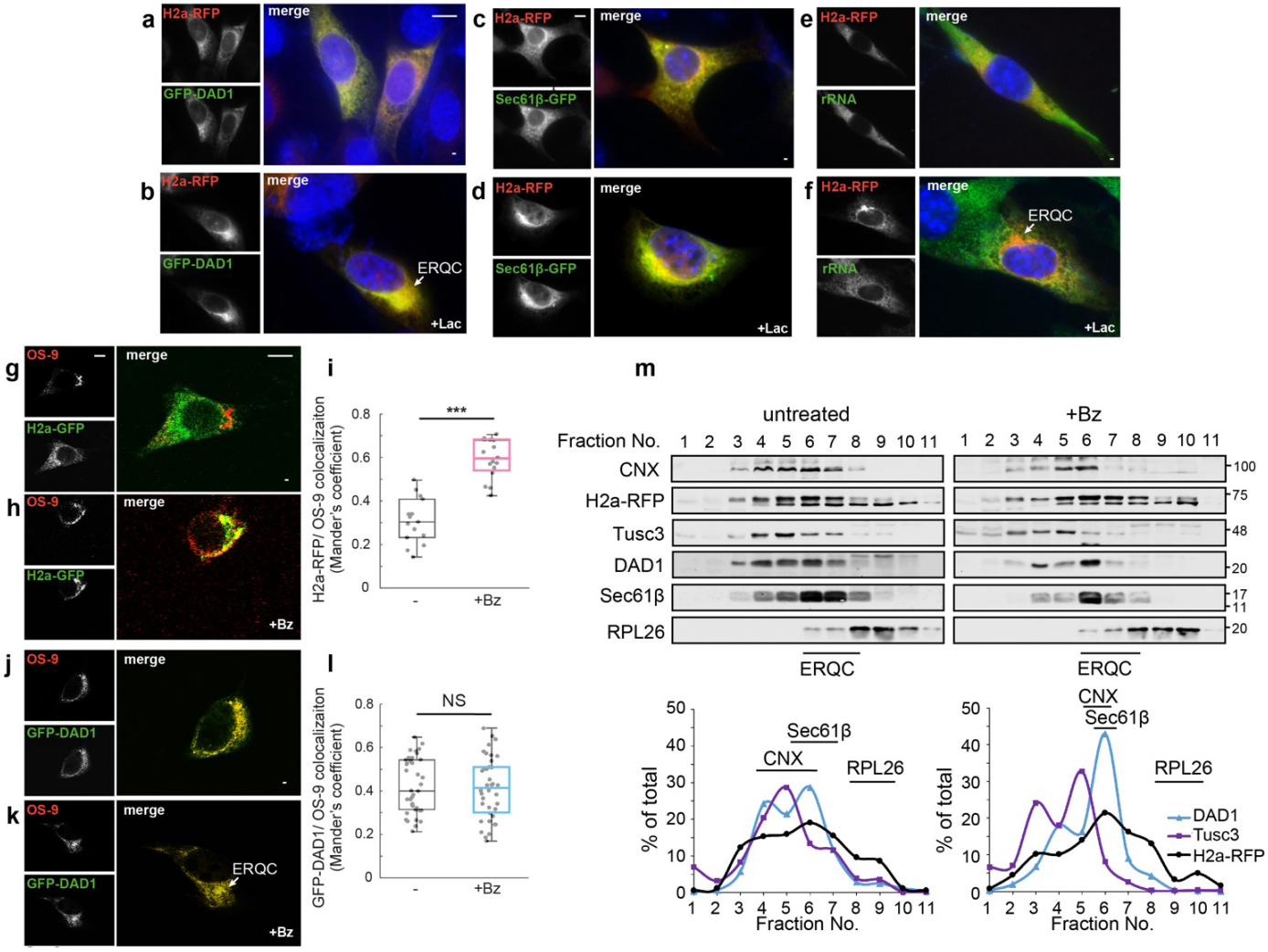
a
H2a-RFP
GFP-DAD1
merge
b
H2a-RFP
GFP-DAD1
merge
ERQC
+Lac
c
H2a-RFP
Sec61β-GFP
merge
d
H2a-RFP
Sec61β-GFP
merge
+Lac
e
H2a-RFP
rRNA
merge
f
H2a-RFP
rRNA
merge
ERQC
+Lac
g
OS-9
H2a-GFP
merge
h
OS-9
H2a-GFP
merge
+Bz
i
***
H2a-RFP/ OS-9 colocalizaiton (Mander's coefficient)
0.8
0.6
0.4
0.2
0
-
+Bz
j
OS-9
GFP-DAD1
merge
k
OS-9
GFP-DAD1
merge
ERQC
+Bz
l
NS
GFP-DAD1/ OS-9 colocalizaiton (Mander's coefficient)
0.8
0.6
0.4
0.2
0
-
+Bz
m
untreated
+Bz
Fraction No. 1 2 3 4 5 6 7 8 9 10 11
CNX
H2a-RFP
Tusc3
DAD1
Sec61β
RPL26
100
75
48
20
17
11
20
ERQC
ERQC
Sec61β
CNX
RPL26
% of total
Fraction No.
CNX
Sec61β
RPL26
DAD1
Tusc3
H2a-RFP
% of total
Fraction No.

Fig. 4

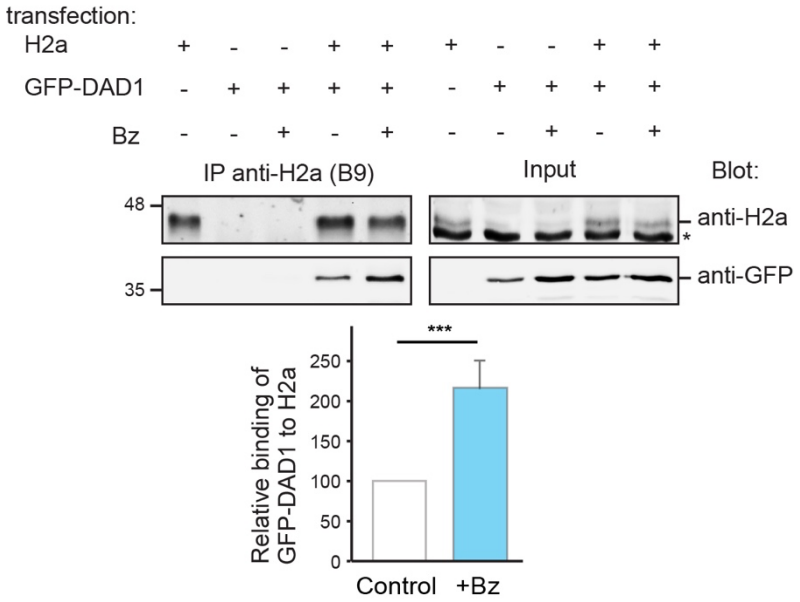

820

821

822

823

824

825

Fig. 5

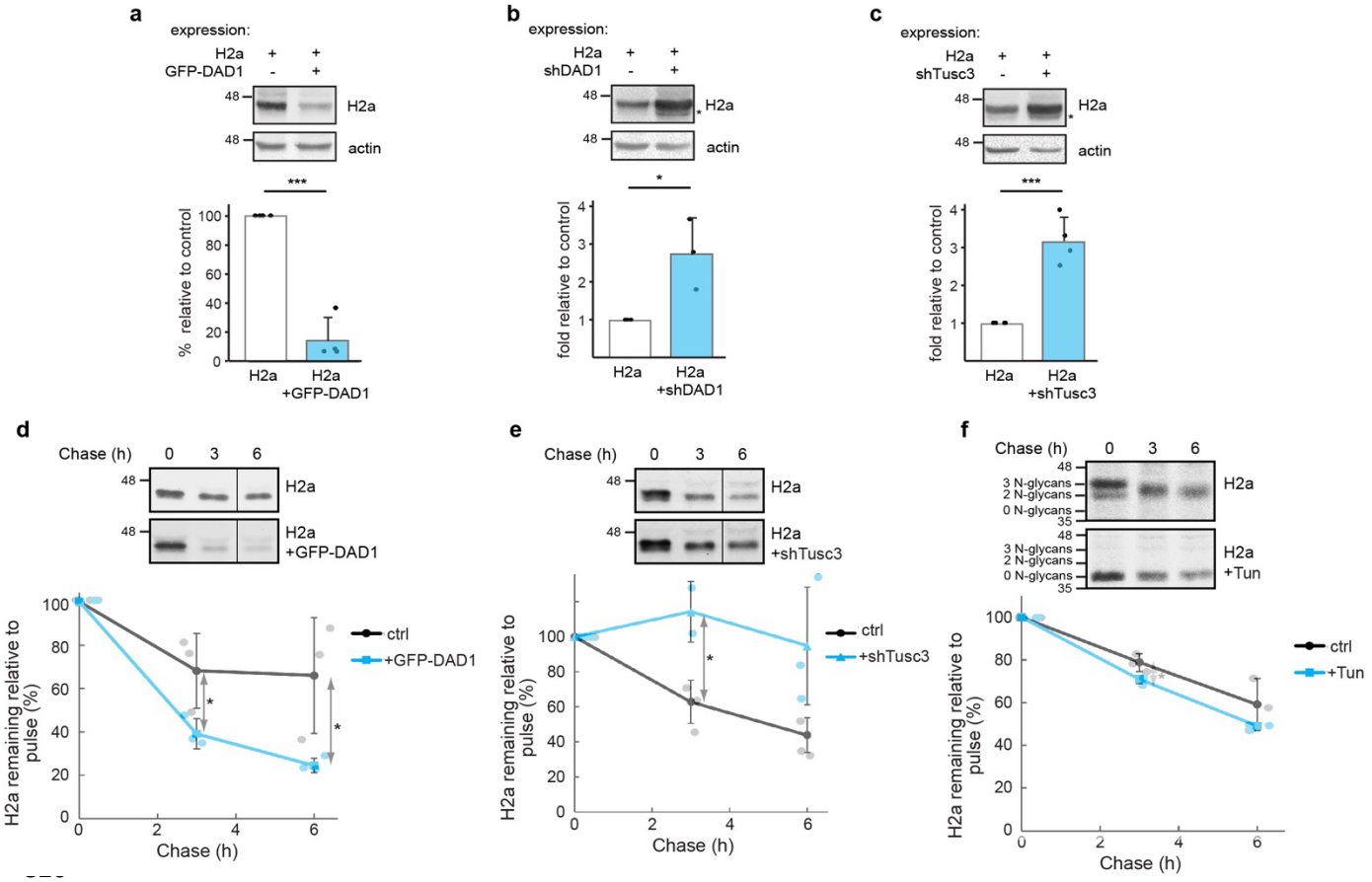
a
expression:
H2a + +
GFP-DAD1 - +
48
H2a
48
actin
***
% relative to control
100
80
60
40
20
0
H2a
H2a +GFP-DAD1
b
expression:
H2a + +
shDAD1 - +
48
H2a
48
actin
*
fold relative to control
4
3
2
1
H2a
H2a +shDAD1
c
expression:
H2a + +
shTusc3 - +
48
H2a
48
actin
***
fold relative to control
4
3
2
1
H2a
H2a +shTusc3
d
Chase (h) 0 3 6
48
H2a
48
H2a +GFP-DAD1
H2a remaining relative to pulse (%)
100
80
60
40
20
0
0 2 4 6
Chase (h)
ctrl
+GFP-DAD1
*
*
e
Chase (h) 0 3 6
48
H2a
48
H2a +shTusc3
H2a remaining relative to pulse (%)
100
80
60
40
20
0
0 2 4 6
Chase (h)
ctrl
+shTusc3
*
f
Chase (h) 0 3 6
48
3 N-glycans
2 N-glycans
0 N-glycans
35
H2a
48
3 N-glycans
2 N-glycans
0 N-glycans
35
H2a +Tun
H2a remaining relative to pulse (%)
100
80
60
40
20
0
0 2 4 6
Chase (h)
ctrl
+Tun

Fig. 6

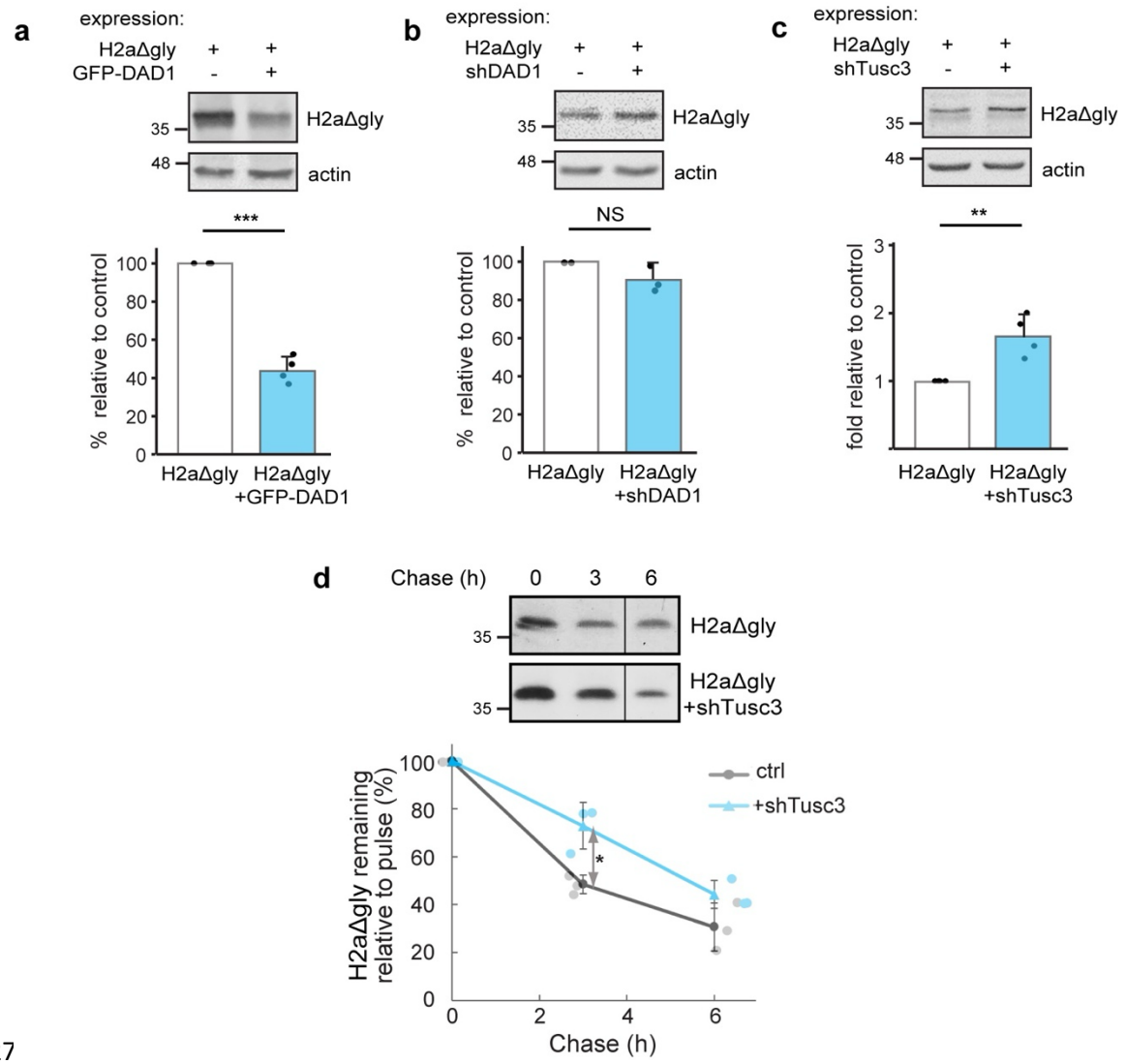

827

828

829

Fig. 7

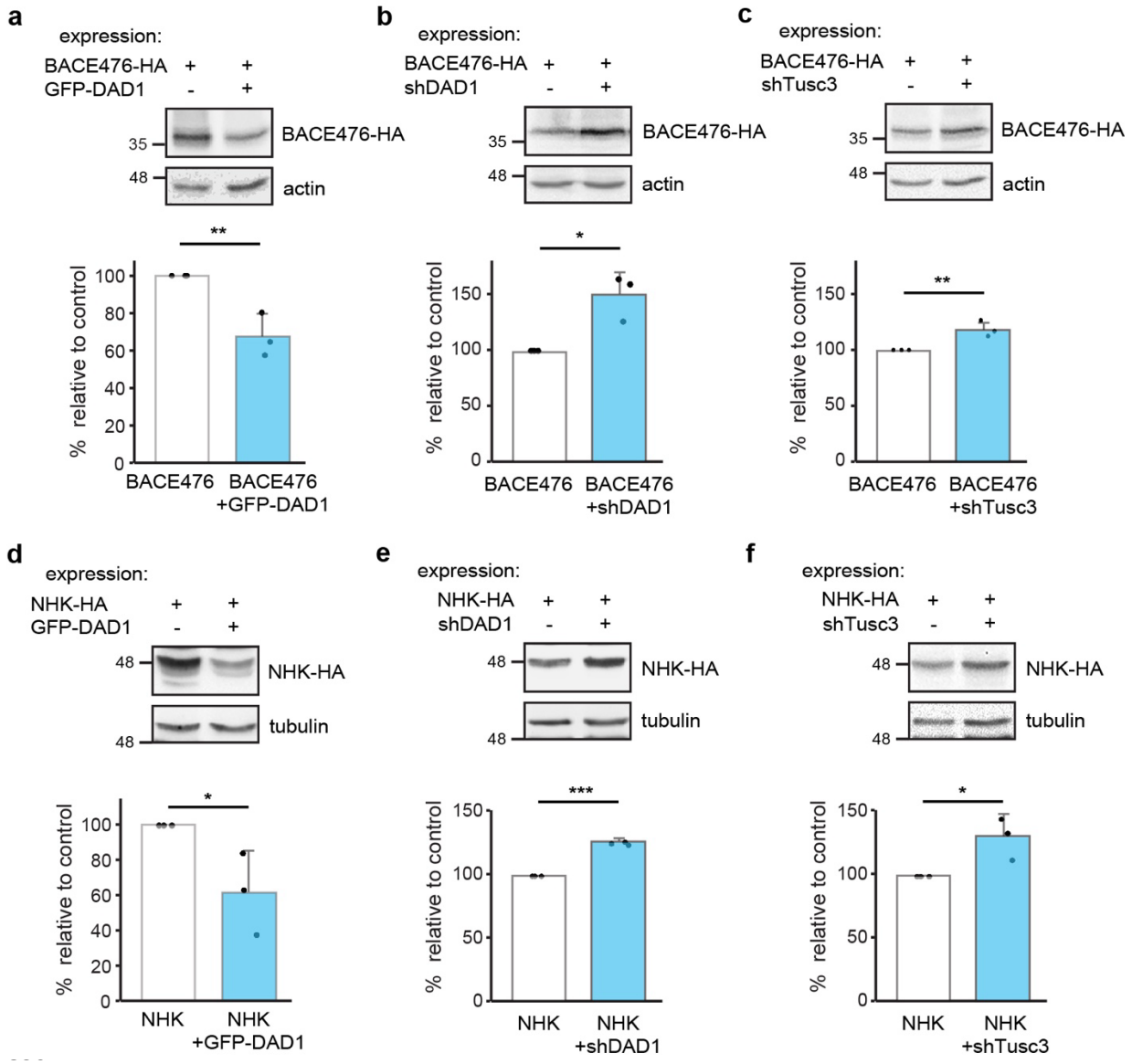

831

832

833

Fig. 8

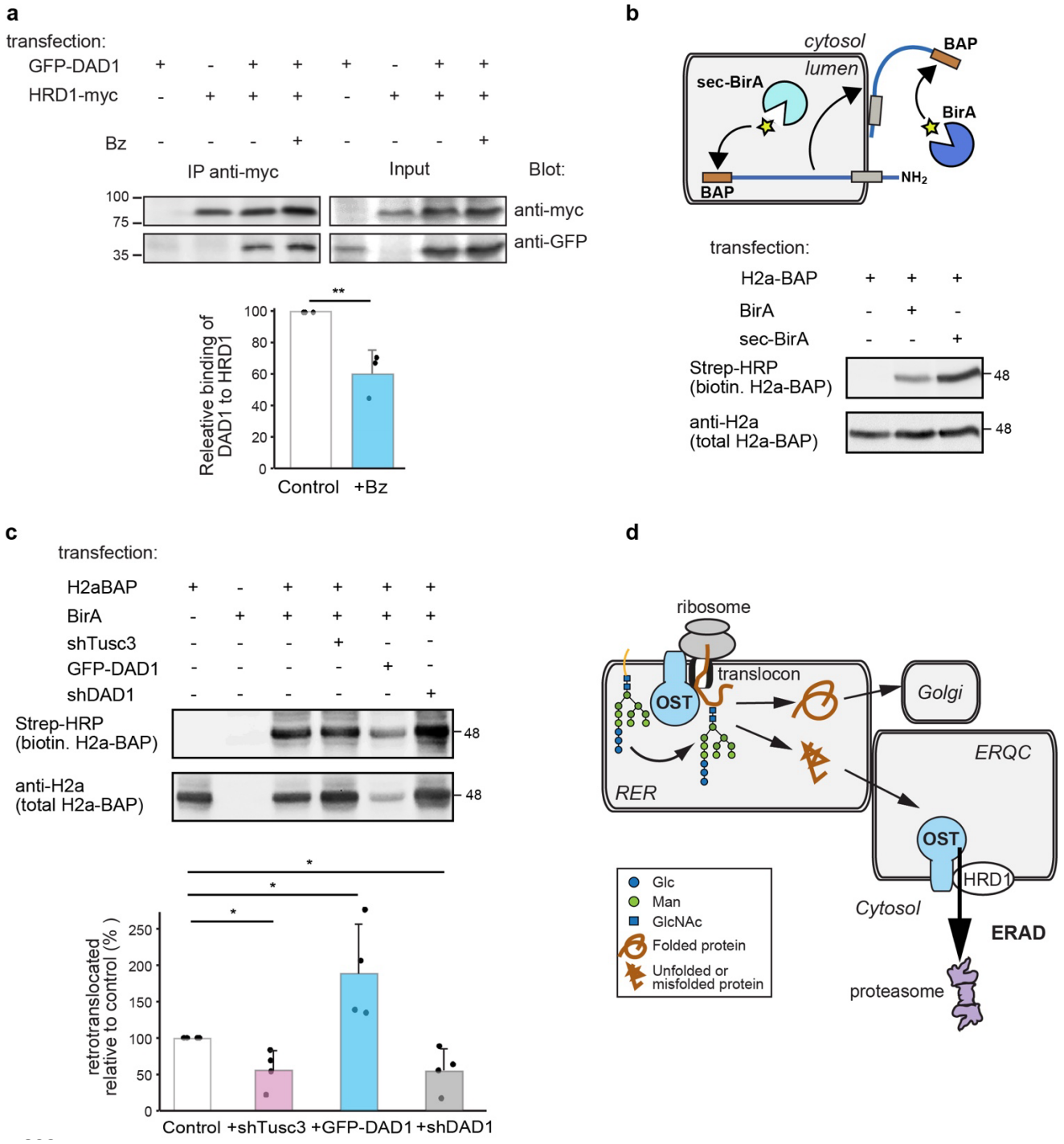
a
transfection:
GFP-DAD1
HRD1-myc
Bz
IP anti-myc
Input
Blot:
100
75
35
anti-myc
anti-GFP
Releative binding of DAD1 to HRD1
Control
+Bz
b
cytosol
lumen
sec-BirA
BAP
BirA
NH2
transfection:
H2a-BAP
BirA
sec-BirA
Strep-HRP (biotin. H2a-BAP)
anti-H2a (total H2a-BAP)
48
c
transfection:
H2aBAP
BirA
shTusc3
GFP-DAD1
shDAD1
Strep-HRP (biotin. H2a-BAP)
anti-H2a (total H2a-BAP)
48
retrotranslocated relative to control (%)
Control
+shTusc3
+GFP-DAD1
+shDAD1
d
ribosome
translocon
OST
Golgi
ERQC
RER
HRD1
Cytosol
ERAD
proteasome
Glc
Man
GlcNAc
Folded protein
Unfolded or misfolded protein